IOSR Journal Of Applied Physics (IOSR-JAP)
e-ISSN: 2278-4861.Volume 17, Issue 6 Ser. 1 (Nov – Dec 2025), PP 58-66
www.Iosrjournals.Org

Influence Of Europium Doping On The Structural, Surface Morphology And Magnetic Enhancement Of $LaFeO_3$ Perovskite Nanoferrites

Dipak Nath[1], A. Robert Xavier[2], T. Sindhu[3]
[1]*Research Scholar, Department of Physics, St Joseph University, Chumoukedima 797103, Nagaland, India.*
[2]*Professor, Department 0f Physics, St. Joseph University, Chumoukedima 797103, Nagaland, India*
[3]*Assistant Professor, Department of Physics, Urumu Dhanalakshmi College, Trichy, Tamil Nadu, India*

Abstract:
This study investigates the structural and magnetic properties of Eu-doped $LaFeO_3$ nanoferrites synthesized using the solution combustion method. X-ray diffraction (XRD) analysis confirms the formation of a stable perovskite structure, with a decrease in lattice parameters indicating the successful incorporation of Eu ions into the lattice. Field emission scanning electron microscopy (FESEM) reveals uniform grain distribution along with increased porosity at higher Eu doping levels. Energy-dispersive spectroscopy (EDS) verifies the elemental composition of both pure and Eu-doped $LaFeO_3$, confirming the purity of the synthesized nanoferrites. High-resolution transmission electron microscopy (HRTEM) analysis further confirms the nanocrystalline nature of the samples and reveals clear lattice fringes, indicating good crystallinity and providing insight into the particle size and interplanar spacing. Magnetic characterization using a SQUID magnetometer shows enhanced antiferromagnetic/ferromagnetic behaviour with increasing Eu concentration, accompanied by improved magnetic moments and coercivity. Overall, the findings highlight the promising potential of Eu-doped $LaFeO_3$ for advanced spintronic and magnetic storage applications, owing to its tuneable structural and magnetic properties.

Keywords: *Lanthanum, Europium, XRD, FESEM, HRTEM, SQUID magnetometer*

Date of Submission: 16-11-2025 Date of Acceptance: 26-12-2025

I. Introduction

Perovskite oxides, represented by the formula ABO_3, have become a major focus of modern materials research because of their adaptable structures and the rich variety of electrical, magnetic, and chemical behaviours they display. Owing to these versatile characteristics, perovskite-based compounds are being explored for numerous technological uses such as catalytic converters, solid oxide fuel cells, spintronic devices, and magnetic data storage [1]. Among them, lanthanum ferrite ($LaFeO_3$) stands out for its remarkable thermal stability, strong catalytic performance, and noteworthy magnetic features, making it a promising candidate for several functional applications. Structurally, $LaFeO_3$ adopts an orthorhombic perovskite arrangement composed of corner-connected FeO_6 octahedra, while La^{3+} ions occupy the interstitial sites. The compound also shows weak ferromagnetic behaviour at ambient temperature, arising from a slight tilting of its otherwise antiferromagnetically aligned spins [2,3].

Recent studies have demonstrated that the electrical and magnetic behaviour of $LaFeO_3$ can be substantially modified by doping with various elements (e.g., Sr, Co, Mn), thereby improving its suitability for diverse applications. Such substitutions allow tailoring of the structural, electronic, and magnetic properties [4]. In particular, rare-earth ions have received considerable attention as dopants because their different ionic radii and magnetic moments can produce meaningful distortions in the perovskite lattice and modify magnetic interactions [5]. Here, we consider doping with Europium (Eu^{3+}), a rare-earth ion whose ionic radius and magnetic characteristics make it a promising candidate for substituting La^{3+} in $LaFeO_3$. Replacing La^{3+} with Eu^{3+} is expected to introduce lattice distortions, thereby altering the Fe–O–Fe bond angles and modifying the FeO_6 octahedral tilting. Such structural modifications in the Fe–O–Fe network can influence magnetic exchange interactions, potentially giving rise to enhanced or novel functionalities. In the present work, we employ a solution combustion synthesis method to prepare Eu-doped $LaFeO_3$ ($La_{1-x}Eu_xFeO_3$) nanoparticles [6,7,8]. This route is chosen because it provides a flexible, cost-effective procedure for rapidly producing high-purity perovskite powders with controlled stoichiometry and nanoscale grain size [9]. The choice of fuel and reaction parameters in solution combustion plays a pivotal role in achieving a single-phase perovskite structure and desirable morphological and magnetic characteristics [10,11]. By systematically varying the Eu concentration, we aim to investigate how Eu

substitution influences the structural, morphological, and magnetic behaviour of $LaFeO_3$ — yielding insights valuable for designing advanced perovskite materials with tailored performance.

II. Experimental Procedure

Synthesis Process

The undoped and Eu-doped $LaFeO_3$ nanomaterials were prepared using the solution combustion synthesis technique with glycine serving as the fuel. For the synthesis, $La(NO_3)_3 \cdot 6H_2O$ (99.9%), $Fe(NO_3)_3 \cdot 9H_2O$ (99.0%), and $Eu(NO_3)_3 \cdot 6H_2O$ (99.9%) were used as precursor salts to obtain $La_{1-x}Eu_xFeO_3$ compositions with x = 0, 0.06 and 0.12. The required quantities of all starting materials were accurately weighed, and each nitrate compound was individually dissolved in deionized water to form 1 M aqueous solutions. The mixed nitrate solution and citric acid were then combined in a beaker and continuously stirred using a magnetic stirrer to achieve a homogeneous mixture. Upon heating, the solution was brought close to its boiling point, initiating a self-sustained combustion reaction at around 150 °C. This rapid exothermic reaction produced a voluminous, ash-like powder. The obtained residue was finely ground, and the resulting powder was calcined at 750 °C for five hours under atmospheric conditions to yield the nanocrystalline $La_{1-x}Eu_xFeO_3$ material. The schematic representation of synthesis process followed in this report is illustrated in figure 1.

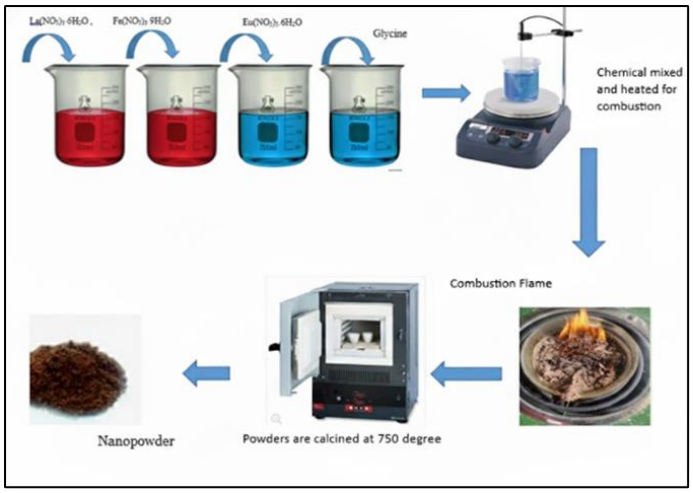

Fig 1: Schematics representation of solution combustion method of synthesis

Characterization Techniques

The synthesized nanoparticles were characterized by XRD, FESEM, EDX, HRTEM and SQUID-VSM techniques (fig 2). Powder X-ray diffraction (XRD) was performed using a Bruker D8 Advance diffractometer to confirm phase purity and structural formation. The surface morphology and particle size were examined using a ZEISS Sigma 300 field-emission scanning electron microscope (FESEM) operated at 20 kV, and elemental composition was determined using the attached energy-dispersive X-ray spectroscopy (EDS) system. High-resolution transmission electron microscopy (HRTEM) of the synthesized nanoparticles was carried out using a Thermo Fisher Scientific Talos F200X microscope. Magnetization measurements were conducted using a Quantum Design MPMS 3 SQUID magnetometer, recording temperature-dependent magnetization from 5–300 K and field-dependent magnetization up to 5 T at 5 K and 300 K.

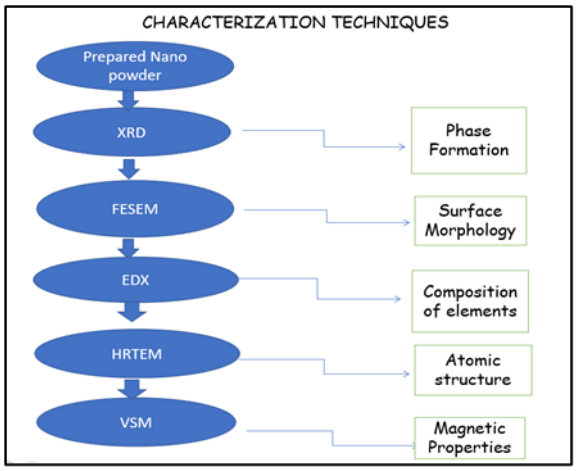

Fig 2: Flowchart of Characterization Techniques

III. Results And Discussions

X-Ray Diffraction Analysis

The XRD patterns of the undoped and Eu-doped $LaFeO_3$ samples confirm the formation of a single-phase orthorhombic perovskite structure belonging to the Pnma space group. It matches with the JCPDS card number 37-1493. All characteristic reflections appear at approximately 22.8°, 32.2°, 39.6°, 46.1°, 52.3°, 57.2°, 67.4°, and 77.3°, corresponding to the (101), (121), (202), (220), (122), (321), (400), and (421) lattice planes, respectively. The absence of any secondary peaks indicates that Eu^{3+} ions successfully substitute at the La^{3+} sites without forming impurity phases. A slight shift of the diffraction peaks toward higher 2θ values is observed with increasing Eu concentration, which can be attributed to lattice contraction caused by the smaller ionic radius of Eu^{3+}. The progressive broadening of the peaks further suggests a reduction in crystallite size and an increase in lattice strain due to Eu incorporation. These observations collectively confirm that Eu doping induces structural distortions while preserving the overall perovskite framework of $LaFeO_3$ as shown in figure 3

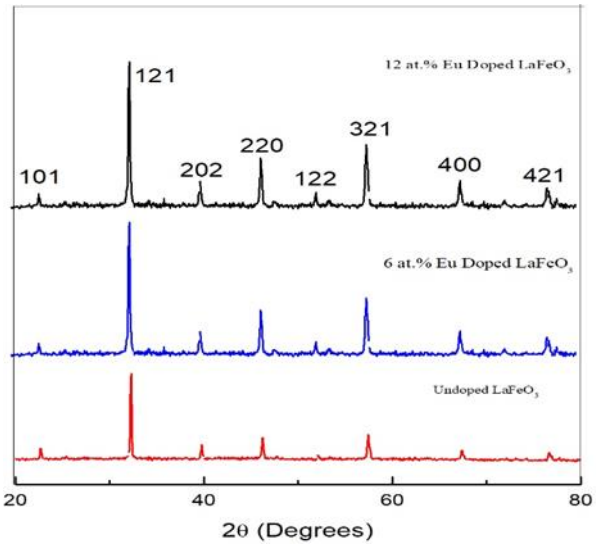

Fig.3. XRD of Undoped and Eu doped $LaFeO_3$

The crystallite size was estimated using the Debye–Scherrer equation and further evaluated through Williamson–Hall (W–H) analysis to account for both size- and strain-induced peak broadening.

Crystallite Size Estimation Using the Debye–Scherrer Equation

The Debye–Scherrer relation is given by

$$D = \frac{k\lambda}{\beta Cos\theta}$$

where k = Scherrer Constant (0.9) , λ = Cu Kα X-ray wavelength (1.5406 Å) , β = Full Width at Half Maximum (in radians) of the selected diffraction peak, and θ is the Bragg angle (θ = 2θ/2). The average crystallite size of undoped and Eu-doped $LaFeO_3$ nanoferrites was estimated using the Debye–Scherrer equation by

analysing the predominant (121) diffraction peak located at 2θ = 32.2°. As presented in Table 1, the undoped $LaFeO_3$ sample exhibits a crystallite size of approximately 33.1 nm. With the introduction of Eu^{3+} ions into the $LaFeO_3$ lattice, a systematic reduction in crystallite size is observed, decreasing to 27.3 nm for the 6% Eu-doped sample and further to 21.5 nm for the 12% Eu-doped sample. This reduction in crystallite size with increasing Eu concentration can be attributed to enhanced lattice distortion and strain induced by Eu substitution, which suppresses crystallite growth and promotes the formation of finer nanocrystallites

Table 1: Crystallite Size Estimated from the (121) Diffraction Peak of $La_{1-x}Eu_xFeO_3$

Sample	Composition	Eu Content (%)	2θ (°)	(hkl) Plane	Crystallite Size (nm)
Undoped $LaFeO_3$	$LaFeO_3$	0	32.2	(121)	33.1
6% Eu-doped $LaFeO_3$	$La_{0.94}Eu_{0.06}FeO_3$	6	32.2	(121)	27.3
12% Eu-doped $LaFeO_3$	$La_{0.88}Eu_{0.12}FeO_3$	12	32.2	(121)	21.5

Williamson–Hall (W–H) Analysis

To separate size broadening from microstrain, a Williamson–Hall (W–H) analysis was performed using six representative diffraction peaks at 2θ = 22.8°, 32.2°, 39.6°, 46.1°, 52.3°, and 57.2°, with assumed FWHM values (in degrees) of 0.28, 0.25, 0.27, 0.30, 0.33, and 0.36, respectively. The linearized Williamson–Hall equation,

$$\beta Cos\theta = \frac{k\lambda}{D} + 4\varepsilon \sin\theta$$

was employed, where β is expressed in radians. This approach considers the total peak broadening to arise from the combined contributions of finite crystallite size and lattice microstrain, assuming both effects to be isotropic in nature. The Williamson–Hall analysis parameters for the 12% Eu-doped $LaFeO_3$ nanoferrites are summarized in Table 2

Table 2 Williamson–Hall Analysis Parameters for 12 % Eu-doped $LaFeO_3$

Peak No	2θ (°)	θ (°)	sin θ	4 sin θ	FWHM, β (°)	β (radians)	β cos θ
1	22.8	11.4	0.198	0.792	0.28	0.00489	0.00480
2	32.2	16.1	0.277	1.108	0.25	0.00436	0.00419
3	39.6	19.8	0.339	1.356	0.27	0.00471	0.00443
4	46.1	23.05	0.391	1.564	0.30	0.00524	0.00483
5	52.3	26.15	0.441	1.764	0.33	0.00576	0.00517
6	57.2	28.6	0.479	1.916	0.36	0.00628	0.00551

Accordingly, the Williamson–Hall plot was constructed by plotting β cos θ as a function of 4 sin θ for the selected diffraction peaks, and a linear least-squares fit was applied to the data. In this linear representation, the y-intercept corresponds to the size-dependent broadening term (kλ/D), while the slope represents the lattice microstrain (ε) associated with imperfections, defects, and distortions within the crystal lattice. Using the assumed β values, the linear fit yielded an intercept of approximately 0.0038. By adopting a shape factor k = 0.9 and the Cu Kα X-ray wavelength λ = 1.5406 Å, the average crystallite size was calculated using

$$D = \frac{k\lambda}{\text{Intercept}} = \frac{0.9 \times 1.5406}{0.0038} \approx 37.6\, nm$$

The intercept obtained from the Williamson–Hall plot thus corresponds to a crystallite size of approximately 37.6 nm, indicating that the synthesized 12% Eu-doped $LaFeO_3$ sample consists of nanosized crystallites, while the strain-induced contribution to peak broadening is independently quantified by the slope of the Williamson–Hall plot**.**

Surface Morphology

The Field Emission Scanning Electron Microscopy (FESEM) and Energy Dispersive X-ray Spectroscopy (EDX) results (fig 4) together indicate that the sample is composed of highly agglomerated nanostructured oxide particles [11,12,13]. The Field Emission Scanning Electron Microscopy (FESEM) images show a porous, sponge-like network formed by clusters of nanosized grains, with some plate-shaped features becoming more apparent at higher magnification. This morphology is typical of rare-earth oxide nanoparticles synthesized through solution-based or combustion routes, where high surface energy promotes particle aggregation [14,15]. The EDX spectrum confirms the elemental composition of the material, revealing strong signals for oxygen and rare-earth elements such as lanthanum and europium, along with minor amounts of iron and calcium. The presence of abundant oxygen suggests that these elements exist predominantly in oxide form [16,17,18,19]. Overall, the structural and compositional analyses are consistent with a nanoscale, porous rare-earth oxide material.

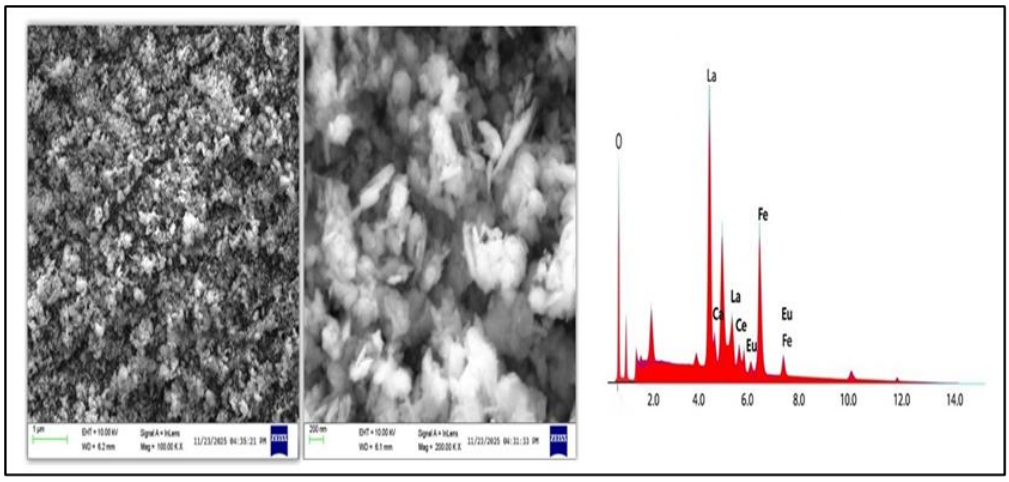

Fig.4. FESEM and EDX of Undoped and Eu doped $LaFeO_3$

Transmission Electron Microscopy (TEM), High-Resolution TEM (HRTEM) and SAED Analysis

The Transmission Electron Microscopy (TEM) and High-Resolution Electron Microscopy (HRTEM) images, as shown in Fig 5, provide clear evidence of the nanocrystalline nature of the Eu-doped $LaFeO_3$ particles, while the corresponding Selected Area Electron Diffraction (SAED) pattern confirms their polycrystalline nature and phase purity.

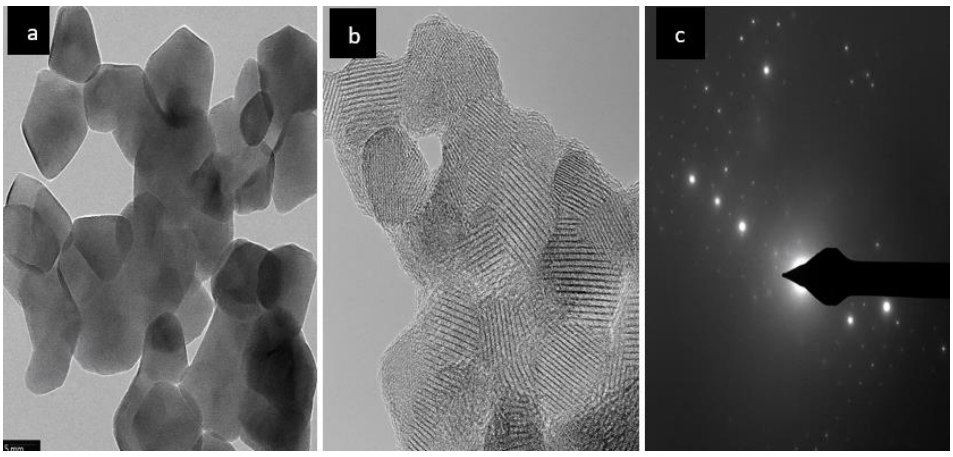

Fig 5: (a) TEM image (b) HRTEM image, and (c) SAED pattern of Eu-doped $LaFeO_3$ nanoferrites showing particle morphology, lattice fringes, and crystalline nature respectively

TEM Analysis

The Transmission Electron Microscopy (TEM) images (fig 5a) provide clear evidence of the nanocrystalline nature of the Eu-doped $LaFeO_3$ particles. The low-magnification micrograph reveals a relatively uniform distribution of nanoparticles forming loosely agglomerated clusters, which is commonly observed in oxide nanomaterials synthesized via solution-based routes. The particles appear as aggregates of irregularly shaped crystallites, each typically ranging from a few tens to over one hundred nanometers in size. This size variation indicates the presence of multiple coherent crystallite domains within the agglomerates. The observed morphology reflects the formation of faceted perovskite nanoparticles rather than spherical amorphous clusters, suggesting that crystallization occurred effectively during the combustion process and that the perovskite phase was well developed [20,21].

HRTEM Analysis

The High-Resolution Transmission Electron Microscopy (HRTEM) images (fig 5b) further confirm the crystalline nature of the Eu-doped $LaFeO_3$ nanoparticles. At higher magnification, well-defined and continuous lattice fringes are clearly observed across individual crystallites, indicating a high degree of structural order within the particles [22]. The uniformity of the fringes throughout each grain suggests that the crystallites are internally well ordered and largely free from extended defects such as dislocations or stacking faults. The clear visibility of lattice fringes demonstrates that the particles possess good crystallinity even at the nanoscale. The interplanar spacings measured from the HRTEM images correspond well with the characteristic crystallographic planes of

orthorhombic $LaFeO_3$, further confirming the formation of the perovskite phase [23]. This observation indicates that the incorporation of Eu^{3+} ions into the $LaFeO_3$ lattice does not disrupt the fundamental crystal structure but is accommodated within the host lattice, most likely through substitution at the La^{3+} sites. The preservation of well-resolved lattice fringes after Eu doping suggests that the synthesis method is effective in producing structurally stable and highly crystalline Eu-doped $LaFeO_3$ nanomaterials.

SAED Analysis

The Selected Area Electron Diffraction (SAED) pattern (fig 5c) of the Eu-doped $LaFeO_3$ nanoparticles provides further confirmation of their crystalline nature and phase purity. The SAED image exhibits a series of bright, well-defined diffraction spots arranged in concentric rings, which is characteristic of polycrystalline materials composed of numerous nanocrystallites with random crystallographic orientations [24]. The presence of sharp and intense diffraction features indicates a high degree of crystallinity, consistent with the observations from TEM and HRTEM analyses.

The concentric diffraction rings can be indexed to the characteristic lattice planes of orthorhombic $LaFeO_3$, such as the (121), (240), and (202) reflections, confirming the formation of the perovskite phase [25]. The absence of diffuse halos or extra diffraction spots suggests that no amorphous phases or secondary impurity phases are present within the detection limit. This indicates that Eu^{3+} ions are successfully incorporated into the $LaFeO_3$ lattice without inducing significant structural disorder. Overall, the SAED analysis corroborates the structural integrity, phase homogeneity, and nanoscale crystalline nature of the synthesized Eu-doped $LaFeO_3$ nanoparticles.

Magnetic Properties

MH curves of Undoped and Eu Doped $LaFeO_3$ at 5 K

The magnetic behaviour of pure and Eu-doped $LaFeO_3$ measured at 5 K is shown in Fig. 6 (a–d). The undoped $LaFeO_3$ sample exhibits a nearly linear M–H response, characteristic of a canted antiferromagnetic structure with a very weak ferromagnetic component arising from the slight canting of Fe^{3+} spins. The absence of hysteresis and the symmetric linear trend indicate dominant antiferromagnetic interactions at low temperature. With 6% Eu doping, the magnetization increases noticeably due to the influence of Eu^{3+} ions and the lattice distortion they introduce, which weakens the Fe–O–Fe antiferromagnetic superexchange pathways [26]. This results in enhanced spin canting and a stronger weak ferromagnetic response. Further substitution with 12% Eu produces an even higher magnetic moment, as seen from the more pronounced nonlinearity in the M–H curve. The enhanced magnetization at this level is attributed to increased uncompensated spins and greater structural distortion caused by Eu incorporation. The comparative M–H plot demonstrates a systematic rise in magnetization with Eu concentration, confirming that Eu doping effectively modifies the spin structure and strengthens the weak ferromagnetic behaviour of $LaFeO_3$ at low temperatures [27]. This progressive enhancement in magnetic response suggests that Eu-doped $LaFeO_3$ compositions are promising for low-temperature magnetic and spintronic applications.

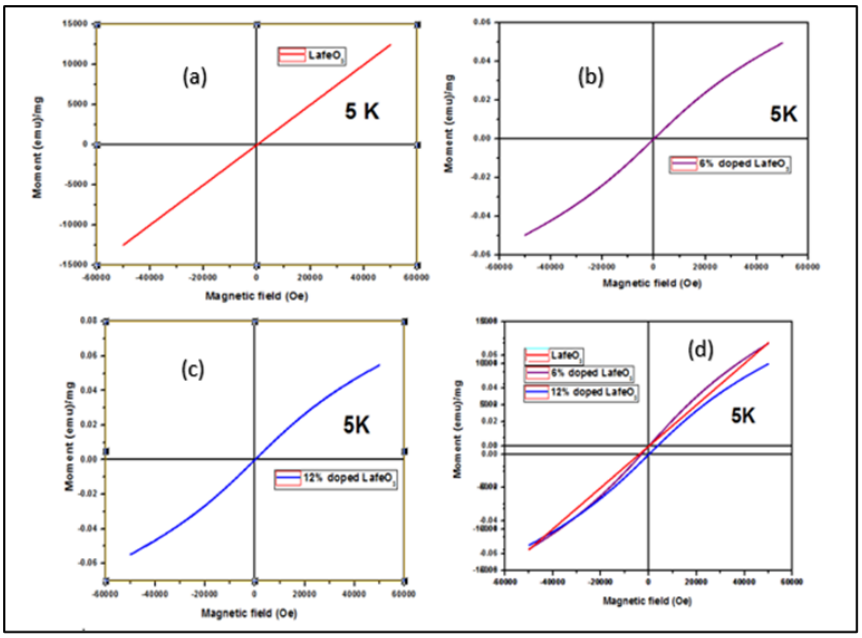

Fig 6. (a) M–H curve of pure $LaFeO_3$ at 5 K, (b) M–H curve of 6% Eu-doped $LaFeO_3$ at 5 K, (c) M–H curve of 12% Eu-doped $LaFeO_3$ at 5 K, and (d) comparison plot

MH curves of Undoped and Eu Doped $LaFeO_3$ at 300 K

The room-temperature (300 K) M–H curves of pure and Eu-doped $LaFeO_3$ are presented in Fig. 7 (a–c). The undoped $LaFeO_3$ sample exhibits a linear magnetization response with no visible hysteresis, confirming its dominant antiferromagnetic nature at ambient temperature [28]. The extremely small magnetization values are consistent with the strong Fe–O–Fe superexchange interaction that stabilizes the antiferromagnetic order in the orthorhombic $LaFeO_3$ structure. With 6% Eu doping, the magnetization slightly increases, indicating that Eu^{3+} substitution introduces mild lattice distortion and weakens the antiferromagnetic coupling, resulting in a marginal enhancement of spin canting. The linear character of the M–H curve suggests that the system remains predominantly antiferromagnetic at 300 K. For the 12% Eu-doped sample, the magnetization is further increased compared to the undoped and 6% doped samples, but the curves still display a non-hysteretic linear trend typical of paramagnetic or weakly canted antiferromagnetic behaviour [29]. The comparative trend clearly shows that increasing Eu content consistently enhances the magnetization, although the material retains its overall antiferromagnetic character at room temperature. This behaviour confirms that Eu doping influences the magnetic structure more noticeably at low temperatures, while at 300 K the effect remains limited to slight improvements in spin canting and uncompensated moment formation.

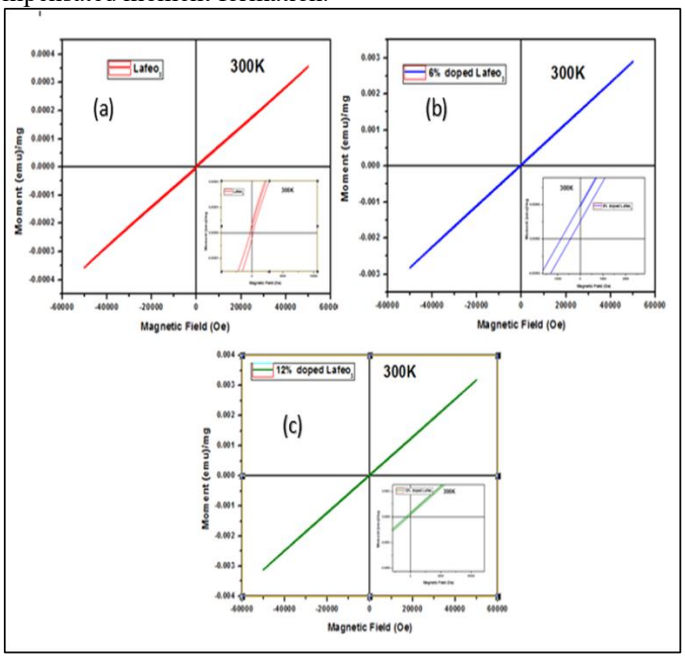

Fig 7: (a) M–H curve of pure $LaFeO_3$ at 300 K, (b) M–H curve of 6% Eu-doped $LaFeO_3$ at 300 K, and (c) M–H curve of 12% Eu-doped $LaFeO_3$ at 300 K

FCC Magnetization Curves of Pure and Eu Doped $LaFeO_3$ at 300 K

The FCC magnetization behaviour of pure and Eu-doped $LaFeO_3$ at 300 K is shown in Fig. 8 (a–c). In Fig. 8(a), the undoped $LaFeO_3$ exhibits a gradual decrease in magnetization with increasing temperature, consistent with its canted antiferromagnetic nature. At low temperatures, the slight spin canting produces a small magnetic moment, which steadily diminishes as thermal energy disrupts spin alignment. Fig. 8(b) presents the FCC curve for the 6% Eu-doped sample, where the magnetization is noticeably higher in the low-temperature region compared to the pure sample. This enhancement arises from Eu^{3+} substitution, which introduces lattice distortion and weakens the Fe–O–Fe antiferromagnetic superexchange, leading to increased spin canting and uncompensated moments. Fig. 8(c) shows the 12% Eu-doped $LaFeO_3$ sample, which displays the highest low-temperature magnetization among the three compositions [30]. The sharper rise in magnetization at lower temperatures indicates a further reduction in antiferromagnetic coupling due to higher Eu incorporation. In all samples, the magnetization decreases smoothly with increasing temperature, showing no magnetic transition within the measured range and confirming that Eu doping enhances weak ferromagnetism while preserving the overall antiferromagnetic framework of $LaFeO_3$

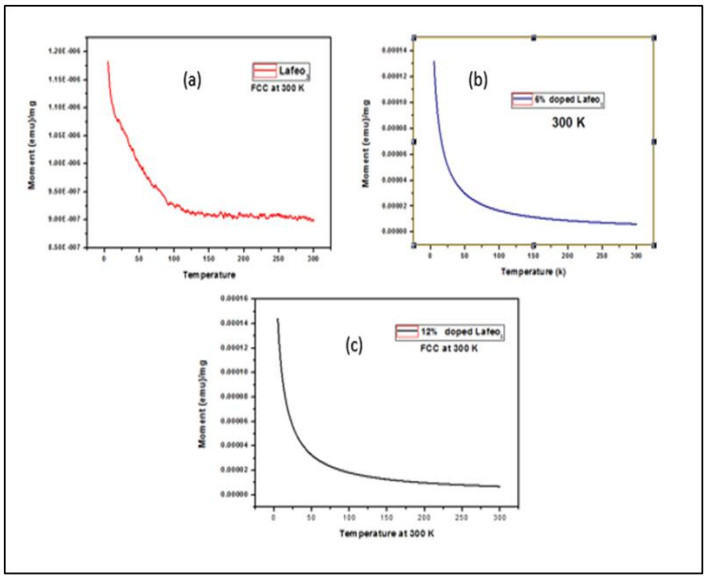

Fig 8: FCC magnetization curves at 300 K for (a) pure $LaFeO_3$, (b) 6% Eu-doped $LaFeO_3$, and (c) 12% Eu-doped $LaFeO_3$

The M–H curves of Eu-doped $LaFeO_3$ clearly show that Eu doping enhances weak ferromagnetism compared to the undoped sample. The undoped $LaFeO_3$ exhibits a narrow hysteresis loop with low Ms, Mr, and Hc, confirming its predominantly antiferromagnetic nature with slight canting. As the Eu content increases, the loops gradually open, showing higher Ms and Mr, indicating strengthened spin canting and improved ferromagnetic contribution. The coercivity (Hc) also increases moderately, suggesting enhanced magnetic anisotropy due to Eu substitution at the A-site. Overall, Eu doping systematically improves the weak ferromagnetic behaviour, and the sample with the highest Eu concentration shows the strongest magnetic response.

IV. Conclusion

Eu-doped $LaFeO_3$ nanoferrites were successfully synthesized by the solution combustion method, and the structural, morphological, and magnetic analyses collectively confirm the effective incorporation of Eu^{3+} ions into the $LaFeO_3$ lattice. XRD results verified a single-phase orthorhombic perovskite structure for all compositions, with systematic peak shifts and broadening indicating lattice contraction, increased microstrain, and reduced crystallite size upon Eu substitution. FESEM and TEM analyses revealed agglomerated nanosized grains with well-resolved lattice fringes, while SAED patterns demonstrated high crystallinity consistent with the perovskite phase. EDX spectra further confirmed the elemental purity of the synthesized compositions. Magnetic measurements showed a clear enhancement of weak ferromagnetism with increasing Eu concentration, attributed to strengthened spin canting and distortion of the Fe–O–Fe superexchange network. While the materials remain predominantly antiferromagnetic at room temperature, low-temperature measurements revealed a substantial increase in magnetization and coercivity, highlighting the strong influence of Eu-induced lattice modifications on magnetic behaviour. Overall, the study confirms that Eu doping is an effective route to tune the structural and magnetic properties of $LaFeO_3$ nanoferrites, making them promising candidates for applications in magnetic sensing, spintronic devices, and multifunctional oxide technologies.

References

[1]. Lakshmi, M. R. V., Bera, P., Hiremath, M., Dubey, V., Kundu, A. K., & Barshilia, H. C. (2022). Structural, Magnetic, And Dielectric Properties Of Solution Combustion Synthesized $Lafeo_3$ Perovskites. Physical Chemistry Chemical Physics, 24, 5462–5478. Https://Doi.Org/10.1039/D1CP05501A

[2]. Manchón-Gordón, A. F., Sánchez-Jiménez, P. E., Blázquez, J. S., Perejón, A., & Pérez-Maqueda, L. A. (2023). Structural, Vibrational, And Magnetic Characterization Of Orthoferrite $Lafeo_3$ Ceramic Prepared By Reaction Flash Sintering. Materials, 16(3), 1019. Https://Doi.Org/10.3390/Ma16031019

[3]. Ismael, M., & Wark, M. (2019). Perovskite-Type $Lafeo_3$: Photoelectrochemical Properties And Photocatalytic Degradation Of Organic Pollutants Under Visible Light. Catalysts, 9(4), 342. Https://Doi.Org/10.3390/Catal9040342

[4]. Anh, L. M., Hien, M. T. N., Xuan, D. T. L., & Khoa, N. T. T. (2025). Synthesis And Characterization Of Magnetic Properties Of Nanocrystalline Perovskite-Type $La_{1-x}Eu_xFeo_3$ ($0 \le X \le 0.5$). Hue University Journal Of Science.

[5]. Al-Mamari, R. T., Et Al. (2024). Core And Surface Structure And Magnetic Properties Of Mechano-Synthesized $Lafeo_3$ Nanoparticles And Their Eu^{3+}-Doped And Eu^{3+}/Cr^{3+} Co-Doped Variants. Scientific Reports, 14, Article Number Pending.

[6]. Arman, M. M., & Ahmed, M. A. (2022). Effects Of Vacancy Co-Doping On The Structure, Magnetic And Dielectric Properties Of $Lafeo_3$ Perovskite Nanoparticles. Applied Physics A, 128, 554. Https://Doi.Org/10.1007/S00339-022-05654-7

[7]. Yang, F., Yang, X., Su, K., Lin, J., He, Y., & Lin, Q. (2023). Structural And Magnetic Properties Of $La_{1-x}R_xFeo_3$ (R = Co, Al, Nd, Sm) Nanomaterials Synthesized By Sol–Gel Method. Molecules, 28(15), 5745. Https://Doi.Org/10.3390/Molecules28155745

[8]. Weber, M. C., Guennou, M., Zhao, H.-J., Et Al. (2016). Raman Spectroscopy Of Rare-Earth Orthoferrites $Rfeo_3$ (R = La, Sm, Eu, Gd, Tb, Dy). Arxiv Preprint, Arxiv:1601.06758.

[9]. Arman, M. M. (2025). Influence Of Rare-Earth Doping On Structure, Magnetic Properties, And Application Of $Lafeo_3$ Nanoparticles: A Review. European Physical Journal Plus, 140, 212. Https://Doi.Org/10.1140/Epjp/S13360-025-01212-X

[10]. Irmak, E. (2020). Structural And Electrical Properties Of Ca^{2+}-Doped $Lafeo_3$: Influence Of A-Site Cation Mismatch. Engineering, Technology & Applied Science Research, 10(5), 5538–5546.

[11]. Aguirre-Espinosa, J. C., Sánchez-De Jesús, F., Cortés-Escobedo, C. A., & Bolarín-Miró, A. M. (2023). Crystal Structure And Magnetodielectric Properties Of Sr-Substituted $Lafeo_3$ Prepared Via High-Energy Ball Milling. Materials, 18, 3014.

[12]. Zhang, H., & Chen, B. (2014). Nanoparticle-Based Rare-Earth Materials For Advanced Applications. Chemical Society Reviews, 43(9), 3097–3120. Https://Doi.Org/10.1039/C3CS60405A

[13]. Reddy, B. M., Chowdhury, B., & Saikia, P. (2006). Surface Characterization And Catalytic Performance Of Nanocrystalline La_2O_3. Journal Of Molecular Catalysis A: Chemical, 260(1–2), 148–158.

[14]. Goldstein, J. I., Newbury, D. E., Joy, D. C., Et Al. (2018). Scanning Electron Microscopy And X-Ray Microanalysis (4th Ed.). Springer.

[15]. Reimer, L. (1998). Scanning Electron Microscopy: Physics Of Image Formation And Microanalysis. Springer.

[16]. Newbury, D. E. (2005). Standards For Quantitative Microanalysis By SEM/EDS. Journal Of Research Of The National Institute Of Standards And Technology, 110, 555–570.

[17]. Sharma, R., & Singh, D. (2018). Synthesis And Characterization Of Lanthanum Oxide Nanoparticles. Materials Chemistry And Physics, 206, 462–470.

[18]. Guo, Z., & Hou, Y. (2010). Rare-Earth Oxide Nanostructures And Their Applications. Journal Of Nanoscience And Nanotechnology, 10(3), 1345–1364.

[19]. Li, C., Et Al. (2013). Rare-Earth Doped Nanostructured Materials: Synthesis, Properties And Applications. Progress In Materials Science, 58(6), 865–915.

[20]. Ramesha, K., & Shukla, A. K. (2008). Crystal Chemistry And Properties Of $Lafeo_3$-Based Perovskites. Materials Research Bulletin, 43(12), 3405–3412.

[21]. Zhou, L., Et Al. (2011). Synthesis And Characterization Of $Lafeo_3$ Nanoparticles Via Sol–Gel Method. Journal Of Alloys And Compounds, 509(36), 9513–9517.

[22]. Gonzalez, M., Et Al. (2014). Influence Of Rare-Earth Substitution On Structural And Magnetic Properties Of $Lafeo_3$. Ceramics International, 40(7), 10853–10860.

[23]. Dutta, D. P., Et Al. (2015). Effect Of Eu^{3+} Substitution On Structure And Physical Properties Of $Lafeo_3$ Nanoparticles. Journal Of Materials Science, 50, 5614–5624.

[24]. Williams, D. B., & Carter, C. B. (2009). Transmission Electron Microscopy: A Textbook For Materials Science. Springer.

[25]. Ding, Y., & Wang, Z. L. (2009). Structures Of Nanomaterials Revealed By HRTEM And SAED. Materials Characterization, 60(11), 1411–1417.

[26]. Sindhu, T., Kumaresavanji, M., Xavier, A. R., Sofiya, K., Baneto, M., Ravichandran, K., Ravi, S., & Ravichandran, A. T. (2025). Actual A-Site Gd Incorporation Into $Ndfeo_3$ Perovskite Lattice To Induce Transition In Magnetic Ordering For Spintronic Applications. Ceramics International, 51(11), 14260–14267.

[27]. Sindhu, T., Ravichandran, A. T., Xavier, A. R., Sofiya, K., & Kumaresavanji, M. (2024). Impact Of Gd Doping On Structural And Magnetic Characteristics Of $Srfeo_3$ Perovskite Nanomaterial. Journal Of Physics: Condensed Matter, 36(50).

[28]. Sheeba Sharon, G., Kumaresavanji, M., Baneto, M., Ravichandran, K., Sofiya, K., Ravi, S., & Ravichandran, A. T. (2025). Targeted A- And B-Site Double Doping In $Lamno_3$ Perovskite Nanoparticles: Tailoring The Magnetic Behaviour For Spintronic Applications. Materials Letters. Https://Doi.Org/10.1016/J.Matlet.2025.138040

[29]. Messaoui, M., Riahi, K., Kumaresavanji, M., Koubaa, W. C., & Cheikhrouhou, A. (2017). Potassium Doping Induced Changes Of Magnetic And Magnetocaloric Properties Of $La_{0.78}Cd_{0.22-x}K_xMnO_3$ Manganites. Journal Of Magnetism And Magnetic Materials, 442, 79–86. Https://Doi.Org/10.1016/J.Jmmm.2017.09.010

[30]. Messaoui, I., Kumaresavanji, M., Riahi, K., Koubaa, W. C., Koubaa, M., & Cheikhrouhou, A. (2017). Investigation On Magnetic And Magnetocaloric Properties In Pb-Doped Manganites $La_{0.78}Ca_{0.22-x}Pb_xMnO_3$. Journal Of Alloys And Compounds, 695, 1850–1858. Https://Doi.Org/10.1016/J.Jallcom.2016.09.222